The Radial Flux HTS Synchronous Motor Stator Windings Comparison for Electrified Aircraft Applications

Zhishu Qiu, Aleksandr Shchukin, Muhammad Bin Younas, Hengpei Liao, Weijia Yuan and Min Zhang

***Abstract*—Electrified aircraft propulsion systems could be a key solution for achieving zero-emission aviation. The need for efficient multi-megawatt motors with high power density makes superconducting motors a promising solution. This study investigates the performance of radial flux high-temperature superconductor (HTS) synchronous motors for electrified aircraft applications, emphasizing the impact of stator windings on power density and losses. In this study, two motor benchmarks of 450 kW and 1 MW are proposed, the impact of an iron core on the stator structure is analyzed, and various stator windings including copper/aluminium Litz wires and HTS coils are compared regarding stator AC loss as well as machine power-to-weight ratio (PTW). The result indicates that air-cored stators are preferred due to their lower weight and reduced losses, particularly in cryogenic conditions. Meanwhile, HTS coils outperform Litz wires at lower cryogenic temperatures (40 K) in terms of machine PTW. At 77 K, however, aluminium Litz wires have an advantage over HTS designs for smaller machines. This study concludes that HTS stators with an air-cored structure can be a desired topology for the future high PTW motor design required in low-emission electrified aviation propulsion systems, especially at low cryogenic temperatures achieved with liquid hydrogen (LH_2).**

***Index Terms*—AC loss, Cryogenic aircraft, Electric aircraft, HTS, Litz wire, Power-to-weight ratio, Radial flux synchronous motor**

I. Introduction

Commercial aviation plays an important role in the evolution and development of society. However, the booming aviation industry is responsible for approximately 2.5% of global CO_2 emissions; currently, its total radiative forcing is above 4% due to significant non-CO_2 effects such as contrail cirrus clouds, induced by water vapor emissions, and emission of indirect greenhouse gases such as NO_x emissions [1], [2], [3], [4], [5]. These figures are expected to rise as air travel increases. This underscores the urgent need for more sustainable aviation technologies. Electrified aircraft propulsion systems are a possible solution to accomplish the goal of zero-emission aviation.

Turboelectric and hybrid electric propulsion are the most promising architectures [6], [7], [8] for large scale electrified aircraft, and their need for efficient multi-megawatt motors with high power density for electrified aircraft makes superconducting motors a potential solution thanks to the high current capability of high temperature superconducting (HTS) materials [2], [3], [9], [10]. Nevertheless, the extra cryogenic cooling system becomes a challenge by adding manufacturing complexity and introducing extra weight.

The adoption of liquid hydrogen (LH_2) is proposed to ease the development of cryogenic superconducting propulsion systems. The main reason is that the very large latent heat of LH_2 makes it sufficient to maintain a superconducting working temperature, and the coolant could be used as cryogenic fuel afterwards. Though there are still many uncertainties of hydrogen electric aircraft regarding increased contrails caused by higher water vapour emissions but the absence of combustion particles, depending on the propulsion strategy (combustion or fuel cell), it could result in an overall reduction in climate impact of 20–25% [11], [12].

HTS machines can be divided into two categories [13]: partially HTS motors with either rotor or stator using HTS materials, and fully HTS motors. Motor designs in the 2010s targeted achieving power-to-weight ratio (PTW) [9], [10] of 10 kW/kg in the short term, 20 kW/kg mid-term, and 50 kW/kg over the long-term respectively. To achieve these ambitious targets, it is important to determine suitable motor topologies. Considering the main losses come from the stator part, it is therefore crucial to determine the stator design.

This study compares the radial flux synchronous motor topology of different HTS motors for aviation applications, highlighting the performance of air-cored designs, the impact of different stator winding technologies, and the specific benefits of HTS stator coils. The comparison focuses on the machine performance of PTW and the stator AC loss. First of all, regarding magnetic loading limits, two motor benchmarks rated at 450 kW (permanent magnet rotor) and 1 MW (HTS magnet rotor) are proposed. The iron core impact on the machine performance is analyzed to explore the features of the air-cored design. In the following part, the HTS stator coil is compared to copper and aluminium Litz structure coils [14], [15] under cryogenic temperatures to investigate the strengths of the HTS stator design. Finally, an in-depth HTS stator coil

This work was supported in part by the Innovate UK Grant Zero Emission Sustainable Transportation (ZEST). *(Corresponding author: Zhishu Qiu).*

Zhishu Qiu, Aleksandr Shchukin, Muhammad Bin Younas, Hengpei Liao, Weijia Yuan and Min Zhang are with the Electronic & Electrical Engineering Department, University of Strathclyde, Glasgow, G1 1XQ UK (e-mail: zhishu.qiu.2018@uni.strath.ac.uk).

Colour versions of one or more of the figures in this article are available online at http://ieeexplore.ieee.org

performance analysis in a machine environment is conducted with the help of FEM (finite element method) simulations in COMSOL Multiphysics.

II. Radial Flux Motor Benchmarks

Though the axial flux motor is desirable because of its compact structure thus high PTW, this design suffers from significant mechanical challenges [16]: Generally, a motor achieves high power density by increasing its rotation speed as fast as mechanically possible. Axial flux motor speed is usually limited by the centrifugal force acting on the rotor which tries to pull it apart. Hence, for high power motor design (such as MW level) in electrified applications, radial flux motors with smaller diameters are preferred due to the lower centrifugal force. As indicated in [17] and [18], to achieve ideal electrical loading for HTS motors, the magnetic loading could be kept under 1 T, which is achievable for both permanent magnet rotors and HTS magnet rotors. Two radial flux motor benchmarks are used for comparison in this study: a 450 kW motor with permanent magnet rotor operating at 77 K, and a 1 MW motor with HTS magnet rotor at 40 K, where 77 K is the temperature using liquid nitrogen (LN_2) as coolant while 40 K is set using LH_2 regarding recent projects of HTS motor design for electric propulsion systems such as the Advanced Superconducting Motor Experimental Demonstrator (ASCEND).

These benchmarks allow the exploration of different stator winding choices and their performance at various temperatures. The detailed benchmark parameters are given in table I.

TABLE I
MOTOR BENCHMARK PARAMETERS

Benchmark	450 kW		1 MW	
Parameter	value	unit	value	unit
Output power	450	kW	1	MW
Input phase voltage	170	Vrms	400	Vrms
Pole pair numeber	6		6	
Mean airgap radius	0.195	m	0.5	m
Stack length	65	mm	100	mm
Rated speed	5000	rpm	5000	rpm
Frequency	500	Hz	500	Hz
Airgap magnetic loading	0.68	T	1	T
Stator working temperature	77	K	77, 40	K

Both motors are designed to operate at a rated speed of 5000 rpm, with an airgap magnetic loading of 0.68 T for 450 KW design and 1 T for 1 MW design. These benchmarks allow for a meaningful comparison between copper/aluminium Litz wire stators and HTS stator coils in terms of power density and losses.

III. Motor Topology Determination

In general, the motor components can be divided into two main categories: active components such as rotor magnets and stator windings and inactive components like the stator core structure. The machine PTW is determined by both types of components. In this study, motor topology determination is mainly focused on the stator part. In this section, the impact of the iron core as well as different types of stator windings on the motor overall loss and the PTW is analyzed.

A. Air-cored Stator Design

First of all, the iron core always adds extra weight, which is not desirable for the high PTW requirement motor design. In addition, this structure produces extra loss. For cryogenic motors, an iron core can introduce additional challenges due to increased hysteresis and eddy current losses. At cryogenic temperatures, iron suffers same amount of hysteresis loss as at room temperature, however, iron experiences 10–20% higher eddy current losses [19] compared to room temperature due to its increased conductivity. Assuming iron loss of 25 kW/kg at 0.7 T and 500 Hz and 50 kW/kg at 1 T and 500 Hz [20], in the 450 kW motor case, this results in 1.5 kW of additional cooling power required, 3–5 kg extra weight, and in the 1 MW motor case, this increases to 3 kW of additional cooling power and 8–12 kg extra weight. These results make an air-cored structure more desirable for high PTW cryogenic motor designs.

B. Stator Winding Comparisons: Analytical AC Loss Analysis

1) **Copper/aluminium Litz wire coil**

Litz wire, a multi-filament wire made of fine, insulated and twisted strands can be used at cryogenic temperature to improve the power density of electrical machines by increasing their current capacity. Cryogenic cooled materials, copper (Cu) and aluminium (Al) for instance, have been proven to achieve current densities as high as 30 A_{peak}/mm^2 at 77 K. Unlike HTS windings which suffer from quenching, cryogenic-cooled Cu/Al Litz wire windings are less sensitive to working temperature under AC conditions. However, the eddy current loss could be a serious problem due to low resistivity and high magnetic field. The total loss in a Litz wire coil is summarized in

$$P_{tot} = P_{rms} + P_{skin} + P_{prox}, \quad (1)$$

where P_{rms} is the coil resistive loss due to transport current, which is independent from the operating frequency, P_{skin} is the skin effect loss and the internal proximity loss (caused by surrounding strands) and P_{prox} indicates the external proximity loss caused by the external field. Considering a Litz wire structure of N strands under a background field strength $\boldsymbol{H}$, the total AC loss [14] could be described in

$$P_{tot} = \frac{R_{dc}\hat{I}^2}{2} + \frac{R_{dc}\hat{I}^2}{2}\left(\frac{N(N-1)}{8}\left(\frac{r_s}{r_L}\right)^2\left(\frac{r_s}{\delta}\right)^4\right) + \frac{N}{8}\omega^2\left(\mu\hat{H}\right)^2\sigma\pi r_s{}^4\ (W/m). \quad (2)$$

The radii of the wire strand, r_s, and of Litz wire, r_L, are set to 0.04 mm and 0.95 mm, respectively, and this strand radius is chosen to ensure that the diameter is less than the skin depth, δ, so that the reaction field due to the eddy currents can be neglected [21], [22]. The material resistivity at cryogenic temperature is considered, and the detailed calculation of resistance, R_{dc}, is given in [14] as well.

2) **HTS coil**

Compared to Litz wire coils, HTS materials have much higher current capacity, especially at lower operating temperatures such as 40 K. Therefore, they show great

potential as stator windings for cryogenic motors. However, under AC conditions, HTS coils experience losses due to the transmitted current and external fields, and their performance depends strongly on the operating temperature and the ratio of the applied current to the critical current. The coil loss due to transport current and a sinusoidal background field is given below [23]:

$$P_{ac} = P_{trans} + P_{mag}, \quad (3)$$

where the transport current loss could be evaluated by [24], [25]:

$$P_{trans} = \frac{\mu_0 f {I_{c0}}^2}{\pi}[a\,ln(a) + (b)\,ln(b) - i^2](W/m). \quad (4)$$

This expression describes the average transport current loss per unit length regarding the Norris equation. If an HTS tape carries an AC current with the amplitude of I_t with the frequency of f, with its self-field critical current, I_{c0}, then the load current ratio, $i = I_t/I_{c0}$, with $a = \mathbf{1} - \boldsymbol{i}$ and $b = \mathbf{1} + \boldsymbol{i}$.

The magnetization loss regarding the Brandt equation [24], [25], [26]:

$$P_{mag} = 4\pi\mu_0 w^2 f H_0 H_c \left\{\frac{2H_c}{H_0} ln[cosh(c)] - tanh(c)\right\}(W/m), \quad (5)$$

with the magnetic strength $H_0 = B_{ext}/\mu_0$ due to the external field B_{ext}; H_c describes the characteristic field generated by $I_{c0}/(2w\pi)$; and $c = \boldsymbol{H_0/H_c}$, then this expression above describes the average magnetization power loss per unit length where the HTS tape has a width of 2 w, and a thickness of h.

A 4 mm YBCO tape is used and its current capacity is assumed to be 50 A_{rms} per tape at 0.68 T and 77 K, and 350 A_{rms} per tape at 1 T and 40 K, respectively, according to information provided by the manufacturer SuperOx [27].

3) Results and discussion

The two benchmarks are set to optimize the performance of Litz wire windings to ensure a fair comparison to HTS windings, which means that HTS stator could be smaller than the stator volume. Regarding AC loss comparison of the three types of windings shown in Fig. 1a, for 450 kW working at 77 K, the HTS coil produces much higher loss than the Cu/Al Litz wire coil, but as the applied current increases, the loss difference reduces. As for the machine PTW ratio comparison, the total machine weight assumptions made here regard the target PTW of short, mid and long term goals. Regarding the PTW result in Fig. 1b, the Al Litz wire design has the best PTW performance, followed by the HTS design and the copper Litz design. The same result could be found in the 1 MW benchmark working at 77 K.

However, a different result is given in the 1 MW benchmark when further reducing the working temperature to 40 K. As shown in Fig. 2, the HTS coil still produces higher loss than the Cu/Al Litz wire coils, however the Al Litz wire generates higher losses than the copper one because of higher eddy current loss due to lower resistivity. Nevertheless, the HTS coil design always has the best PTW performance, especially if the machine weight can be reduced below 50 kg.

Therefore, regarding machine PTW, the advantage of an HTS stator over Litz wire structure happens when the cryogenic temperature is low enough for the HTS structure to show its superior current capacity.

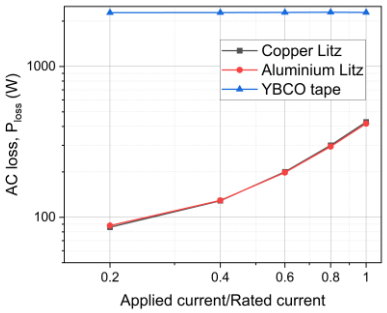

(a)

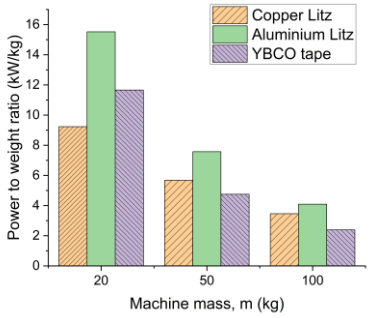

(b)

Fig. 1. Stator winding comparison for 450 kW benchmark at 77 K a) AC loss, b) Power density.

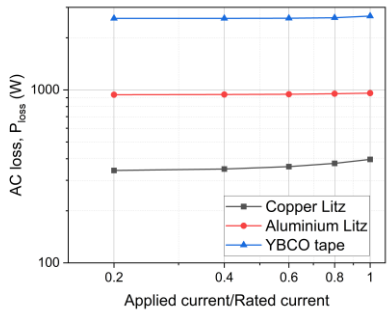

(a)

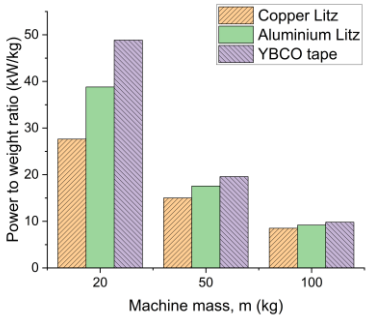

(b)

Fig. 2. Stator winding comparison for 450 kW benchmark at 40 K, 1 T a) AC loss, b) Power density.

<

IV. Improved HTS Insulated Stator Coil AC Loss Simulations

A. HTS coil preparation and simulation validations

A 68 turn (34 turn per layer) double pancake sample coil wound from SuperOx 2G YBCO tapes is made to further analyze the AC loss performance of insulated HTS coils under a real motor environment. The tape width is 4 mm, with inner and outer diameters of 60 mm and 85 mm, respectively; and for each coil turn, the copper stabilizer around each tape is about 20 µm thickness. The coil self-field, I_c, is 80 A at 77 K.

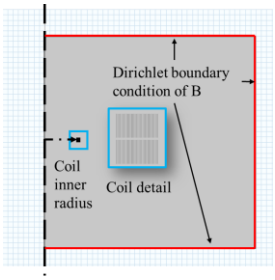

Fig. 3. Coil simulation model geometry of one side of the coil.

A 2D Cartesian coordinate model using the H-formulation is built for numerical analysis. The geometry of one side of the coil is illustrated in Fig. 3. Regarding the studies in [28], it is reasonable to simplify the tape structure by modelling only the 2 µm YBCO layer. In 2D cartesian coordinates, the current J_z flows along the z direction, while the two magnetic field variables, $\boldsymbol{H} = [H_x; H_y]$ are in the *x*-*y* plane. The relationship between the current and magnetic field is obtained by the original Ampère's law. By substituting magnetic field and electric field variables into Faraday's law for cylindrical coordinates:

$$\begin{bmatrix} \frac{\partial E_z}{\partial y} \\ -\frac{\partial E_z}{\partial x} \end{bmatrix} = -\mu_r \mu_0 \begin{bmatrix} \frac{\partial H_x}{\partial t} \\ \frac{\partial H_y}{\partial t} \end{bmatrix}. \quad (6)$$

To improve the AC loss evaluation, rather than using constant critical current density, J_c, an external field dependent $J_{c(\theta,B)}$ is introduced and is taken from interpolation data of same samples. Meanwhile, the *E*-*J* power law is used to describe the non-linear resistivity of HTS materials:

$$\rho = \frac{E_0}{J_c(\theta,B)} \times \left(\frac{J}{J_c(\theta,B)}\right)^{n-1}. \quad (7)$$

Initially, the coil self-field critical current calibration was achieved with the help of measurement. Fig. 4 shows the transport current loss simulation validation at 50, 75 and 100 Hz. It shows good consistency.

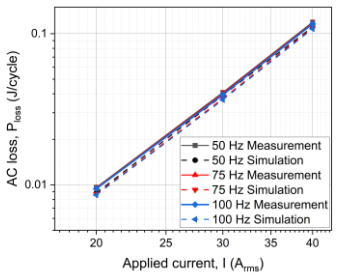

Fig. 4. Coil AC loss Simulation model validation.

B. HTS coil AC loss evaluation in machine environment

The coil under a rotating magnetic field of 0.68 T is simulated at 40, 65 and 77 K and the result is given in Fig. 5, where the magnetic field distribution is extracted from a radial flux motor design. The applied current range for each temperature is limited by the critical current. It is interesting to find that the magnetization loss increases with reducing temperature. To further analyze the AC loss variation, the current penetration of the magnetization loss at each of the three temperatures is shown in Fig. 6. It indicates that the magnetic field penetrates more easily and uniformly, thus reducing the hysteresis loop [29] as the temperature increases, leading to a more efficient distribution of the field and reduced localized loss. The total loss dominant component transfers from magnetization loss to transport current loss as the applied current increases. The total loss increases dramatically as the applied current reaches I_c. To avoid dominant magnetization and to maximize HTS current capacity utilization, a current close to but below its I_c is desired.

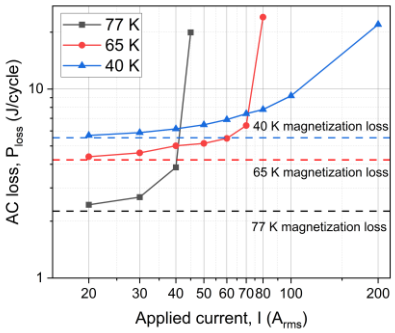

Fig. 5. AC loss simulation results at 40, 65, and 77 K under a rotating field of 0.68 T.

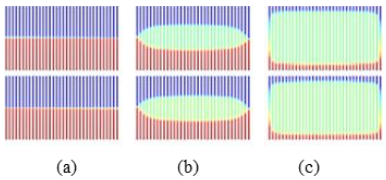

Fig. 6. Coil current penetration at one twentieth of period: a) 77 K, b) 65 K and c) 40 K respectively.

V. Conclusion

This study compared stator designs of a radial flux synchronous motor in electrified applications focusing on the stator iron impact and the stator winding choices. An air-cored structure is desirable for cryogenic motor design for electrified aircraft as iron can introduce extra weight and losses. For a 450 kW level machine, under 77 K, the aluminium Litz wire stator performs the best considering both stator loss and the machine PTW; while for a 1 MW level machine, under 40 K, the HTS coil shows higher PTW especially if the machine weight is under 50 kg. In addition, with the help of the simulation analysis of a small insulated HTS coil, to maximize the high current capacity of HTS coils, a high current close to its I_c is desirable. Future work should focus on optimizing the design and cooling strategies, and evaluate machine power density considering both the machine weight and volume.

REFERENCES

[1] H. Ritchie, "What share of global CO_2 emissions come from aviation?" *Our World in Data*, 2024. [Online]. Available: https://ourworldindata.org/global-aviation-emissions

[2] Y. Wang, C. Zhang, C. Zhang, and L. Li, "Review of high-power-density and fault-tolerant design of propulsion motors for electric aircraft," *Energies*, vol. 16, no. 19, p. 7015, 2023.

[3] "*Aviation: Benefits beyond borders global report*," Air Transport Action Group, Geneva, Switzerland, Rep. 2020.

[4] A. Boglietti, A. Cavagnino, A. Tenconi, S. Vaschetto, and P. di Torino, "The safety critical electric machines and drives in the more electric aircraft: A survey," in *IECON 2009*, Nov. 3–5, 2009, pp. 2587–2594.

[5] D. S. Lee et al., "The contribution of global aviation to anthropogenic climate forcing for 2000 to 2018," *Atmospheric Environment*, vol. 244, 2021, doi: https://doi.org/10.1016/j.atmosenv.2020.117834.

[6] M. Armstrong, "Superconducting Turboelectric Distributed Aircraft Propulsion," in *Proc. Cryogenic Eng. Conf/Int. Cryogenic Mater. Conf.*, p. 34, 2015.

[7] B. J. Brelje, J. R. Martins, Electric, hybrid, and turboelectric fixed-wing aircraft: A review of concepts, models, and design approaches. *Progress in Aerospace Sciences*, 104, 1–19, 2019.

[8] C. Hartmann, J. K. Nøland, R. Nilssen, and R. Mellerud, "Dual use of liquid hydrogen in a next-generation PEMFC-powered regional aircraft with superconducting propulsion," *IEEE Transactions on Transportation Electrification*, vol. 8, no. 4, pp. 4760–4778, Dec. 2022, doi: 10.1109/TTE.2022.3170827.

[9] P. Wheeler and S. Bozhko, "The more electric aircraft: Technology and challenges," *IEEE Electrification Magazine*, vol. 2, no. 4, pp. 6–12, 2014, Art no. 7008830, doi: 10.1109/MELE.2014.2360720.

[10] National Academies of Sciences and Medicine, *Commercial aircraft propulsion and energy systems research: Reducing global carbon emissions*. Washington, DC: The National Academies Press (in English), 2016, p. 122.

[11] F. Yin, V. Grewe, K. Gierens, Impact of hybrid-electric aircraft on contrail coverage. *Aerospace*, vol. 7, no. 10, p. 147, 2020.

[12] A. Rap, W. Feng, P. Forster, D. Marsh, and B. Murray, "The climate impact of contrails from hydrogen combustion and fuel cell aircraft", *EGU General Assembly 2023*, Vienna, Austria, 23–28 Apr 2023. EGU23-5520, https://doi.org/10.5194/egusphere-egu23-5520, 2023.

[13] K. S. Haran et al., "High power density superconducting rotating machines—development status and technology roadmap," *Superconductor Science and Technology*, vol. 30, no. 12, p. 123002, 2017/11/17 2017, doi: 10.1088/1361-6668/aa833e.

[14] C. D. Manolopoulos, M. F. Iacchetti, A. C. Smith, P. Miller, and M. Husband, "Litz wire loss performance and optimization for cryogenic windings," *IET Electric Power Applications*, vol. 17, no. 4, pp. 487–498, 2023/04/01 2023, doi: https://doi.org/10.1049/elp2.12279.

[15] New England Wire Technologies, *Traditional Litz wire theory*. (2025). [Online]. Available: https://www.newenglandwire.com/wire-and-cable-101/

[16] P. Leijnen, *The Practice: Resolving the Challenges*. (2024) [online]. Available: https://traxial.com/blog/the-practice-resolving-the-challenges/.

[17] R. Mellerud, C. Hartmann, C. L. Klop, S. Austad, and J. K. Nøland, "Design of a power-dense aviation motor with a low-loss superconducting slotted armature," *IEEE Transactions on Applied Superconductivity*, vol. 33, no. 8, pp. 1–13, 2023, doi: 10.1109/TASC.2023.3316192.

[18] M. Corduan, M. Boll, R. Bause, M. P. Oomen, M. Filipenko, and M. Noe, "Topology comparison of superconducting AC machines for hybrid electric aircraft," *IEEE Transactions on Applied Superconductivity*, vol. 30, no. 2, pp. 1–10, 2020, doi: 10.1109/TASC.2019.2963396.

[19] M. Miyamoto, T. Matsuo, and T. Nakamura, "Measurement of vector hysteretic property of silicon steel sheets at liquid nitrogen temperature," *Przegląd Elektrotechniczny*, vol. 87, no. 9b, pp. 111–114.

[20] Cogent Power (2011), *Non oriented electrical steel*, [Online]. Available: https://emagnetica.pl/database-em/01_Soft/Electrical_steels/Cogent_Newport_2003/NO-11.pdf.

[21] A. W. Lotfi and F. C. Lee, "A high frequency model for Litz wire for switch-mode magnetics," in *Conference Record of the 1993 IEEE Industry Applications Conference Twenty-Eighth IAS Annual Meeting*, 2–8 Oct. 1993, pp. 1169–1175 vol. 2, doi: 10.1109/IAS.1993.299045.

[22] J. Acero, P. J. Hernandez, J. M. Burdio, R. Alonso, and L. A. Barragdan, "Simple resistance calculation in litz-wire planar windings for induction cooking appliances," *IEEE Transactions on Magnetics*, vol. 41, no. 4, pp. 1280–1288, 2005, doi: 10.1109/TMAG.2005.844844.

[23] J. R. Bumby, *Superconducting Rotating Electrical Machines*. Oxford: Clarendon Press, 1983.

[24] H. Zhang, P. Machura, K. Kails, H. Chen, and M. Mueller, "Dynamic loss and magnetization loss of HTS coated conductors, stacks, and coils for high-speed synchronous machines," *Superconductor Science and Technology*, vol. 33, no. 8, p. 084008, 2020, doi: 10.1088/1361-6668/ab9ace.

[25] E. H. Brandt and M. Indenbom, "Type-II-superconductor strip with current in a perpendicular magnetic field," *Physical Review B*, vol. 48, no. 17, pp. 12893–12906, 1993, doi: 10.1103/PhysRevB.48.12893.

[26] M. R. Halse, "AC face field losses in a type II superconductor," *Journal of Physics D: Applied Physics*, vol. 3, no. 5, p. 717, 1970, doi: 10.1088/0022-3727/3/5/310.

[27] S. Wimbush, N. Strickland, A. Pantoja (2016) *A high-temperature superconducting (HTS) Wire Critical Current Database*, [online] Available: https://figshare.com/collections/A_high_temperature_superconducting_HTS_wire_critical_current_database/2861821.

[28] M. Zhang, J.-H. Kim, S. Pamidi, M. Chudy, W. Yuan, and T. A. Coombs, "Study of second generation, high-temperature superconducting coils: Determination of critical current," *Journal of Applied Physics*, vol. 111, no. 8, p. 083902, 2012, doi: 10.1063/1.3698317.

[29] M. P. Oomen, "AC loss in superconducting tapes and cables," Ph.D. dissertation, Dept. EMS, Fac. Sci. and Tech., Univ. of Twente, Enschede, Netherlands, 2000.